Analysis of the effect of local interactions on protein stability

Victor Muñoz, Philippe Cronet, Eva López-Hernández and Luis Serrano

Background: Protein stability appears to be governed by non-covalent interactions. These can be local (between residues close in sequence) or non-local (medium-range and long-range interactions). The specific role of local interactions is controversial. Statistical mechanics arguments point out that local interactions must be weak in stable folded proteins. However, site-directed mutagenesis has revealed that local interactions make a significant contribution to protein stability. Finally, computer simulations suggest that correctly folded proteins require a delicate balance between local and non-local contributions to protein stability.

Results: To analyze experimentally the effect of local interactions on protein stability, each of the five Che Y α-helices was enhanced in its helical propensity. α-Helix-promoting mutations have been designed, using a helix/coil transition algorithm tuned for heteropolypeptides, that do not alter the overall hydrophobicity or protein packing. The increase in helical propensity has been evaluated by far-UV CD analysis of the corresponding peptides. Thermodynamic analysis of the five Che Y mutants reveals, in all cases, an increase in half urea ($[\text{urea}]_{1/2}$) and in Tm, and a decrease in the sensitivity to chemical denaturants (m). ANS binding assays indicate that the changes in m are not due to the stabilization of an intermediate, and the kinetic analysis of the mutants shows that their equilibrium unfolding transition can be considered as following a two-state model, while the change in m is found in the refolding reaction (m_{kf}).

Conclusions: These results are explained by a variable two-state model in which the changes in half urea and Tm arise from the stabilization of the native state and the decrease in m from the compaction of the denatured state. Therefore, the net change in protein stability in aqueous solution produced by increasing the contribution of native-like local interactions in Che Y is the balance between these two conflicting effects. Our results support the idea that optimization of protein stability and cooperativity involve a specific ratio of local versus non-local interactions.

Introduction

The thermodynamic analysis of small monodomain proteins has shown that the behaviour of these proteins can usually be described as an equilibrium between two states, folded and unfolded, with a very cooperative transition between them [1]. Protein stability is defined, therefore, as the difference in free energy between the folded (native) and the unfolded state. This difference in free energy, which under physiological conditions is small and in favour of the folded (native) state, arises from the difference between two large numbers: the factors stabilizing the folded state and those stabilizing the unfolded state [2]. The major contribution to stabilization of the folded state appears to be the set of non-covalent interactions between protein residues that take place in this conformation [3], whereas the unfolded state is mainly stabilized by its large conformational entropy. Quantification of the interaction energies is, therefore, essential to understanding protein stability. Quantification has been attempted

experimentally by the use of protein engineering procedures combined with physico-chemical techniques and the knowledge of high-resolution protein three-dimensional structures. In fact, several groups have been using this strategy extensively to study the effect on stability of a large variety of mutations [4,5].

An important puzzle in protein stability stems from the relative contribution of interactions between residues close together in the sequence (local interactions), compared to the contribution of those between residues further apart in the sequence (medium-range and long-range interactions). Local interactions appear to be involved in defining the secondary structure, whereas non-local interactions form the tertiary structure. However, the specific role of each type of interaction on protein stability is not as yet known. Statistical mechanics arguments suggest that the smaller the distance between residues in the sequence, the lower the specificity for the

folded conformation and, thus, the lower the net contribution to protein stability. On this basis, it has been proposed that non-local interactions are essential for providing the specificity required for protein stability, whereas local interactions play only a marginal role [3,6]. Computer simulations have found that there should be an optimal ratio of local versus non-local contributions [7–9]. Values over the upper limit lead to molten globule like proteins and values under the lower limit give proteins that are compact but do not have defined secondary structure [9]. The experimental information available on the contribution of local interactions to protein stability is somewhat controversial. Secondary structure propensities of protein fragments are low in most of the cases studied [10], suggesting that local interactions are weak. On the other hand, site-directed mutagenesis experiments have indicated the existence of different secondary structure propensities for the 20 amino acids, both for α-helices [11–13] and β-strands [14–16], with differences of more than 1 kcal mol^{-1} in some cases. Moreover, it has been shown that substitution of the α-helix C of ribonuclease A by derivatives with increased helical content results in semisynthetic ribonucleases with higher thermal stability [17]. Several groups have also performed alanine substitutions in helical positions of different proteins, which generally convey small increases in protein stability [18,19].

In this work, we seek to analyze in more detail the extent to which local interactions contribute to protein stability. Particularly, we investigate experimentally the concept of the optimal ratio between local and non-local contributions to protein stability. For this, we have devised an experiment in which the helical propensity of each of the five Che Y α-helices is enhanced by local interactions. The effect on protein stability is determined from the thermodynamic analysis of Che Y mutants bearing each of the enhanced α-helices. A crucial step in this experiment is the design of mutations that enhance helical propensities, and this was carried out on the basis of the following principles. First, the target sites for mutagenesis were selected in each α-helix as those fully solvent exposed positions in which the sidechain does not interact with residues not included in the α-helix (see Fig. 1). The intention is to guarantee that the protein packing is maintained and that the mutations do not eliminate medium-range or long-range interactions. Second, selection of a target site requires that it is occupied by a non-hydrophobic residue (residues other than Leu, Ile, Val, Met, Phe, Tyr, and Trp) in the wild-type Che Y. This ensures that the overall hydrophobicities of the mutant proteins and wild-type Che Y are similar. Third, the mutations are designed to enhance α-helix propensity as indicated by a helix/coil transition algorithm tuned for heteropolypeptides [20] and considering only polar to polar or polar to alanine changes. Mutations involving glycine residues are avoided to eliminate effects arising from its different conformational entropy, and mutations to alanine are minimized to avoid unnecessary changes in overall hydrophobicity. Having designed the mutations, the putative increases in helical propensity were evaluated by far-UV CD analysis of short synthetic peptides and the effects on protein stability were determined by the thermodynamic analysis of the mutant proteins.

Results

As a template for the experiment, we have used a recombinant version of *Escherichia coli* Che Y [21] with the mutation Phe14→Asn. The effect of this mutation has been characterized in detail and found to increase stability in aqueous solution and to destabilize the kinetic intermediate (pseudo-wild-type) [22]. Destabilization of this kinetic intermediate allows the kinetic data to be fitted to a two-state model in the urea concentration range 3–10 M (V Muñoz, E López-Hernández, L Serrano, unpublished data). Site-directed mutagenesis and protein purification was performed as previously published [21].

Design of mutations

Mutations were designed following the principles detailed in the Introduction. We used a modified version of the helix/coil transition algorithm AGADIR [20] that includes a multiple sequence approximation (AGADIRms; V Muñoz, L Serrano, unpublished data). In this version, helical populations of the residues in the molecule are normalized with the complete molecular partition function. We identified the limits of the five α-helices using the crystallographic coordinates of the wild-type Che Y [23] and the algorithm of Kabsch and Sander [24]. The target sites in each α-helix were those positions with an amino acid other than Leu, Ile, Val, Met, Phe, Tyr, and Trp, more than 90% solvent accessibility as calculated with the algorithm of Lee and Richards [25], and without groups from other protein regions closer than 6 Å to any atom of the target sidechains. The designed helix 1 (Hel1) incorporates the mutations Thr16→Ala, Arg19→Glu, and Asn23→Arg (Fig. 1b). Designed helix 2 (Hel2) incorporates the mutations Gly39→Ala, Asp41→Glu, and Asn44→Arg (Fig. 1c). Gly39 is almost completely buried (15% solvent accessibility) and its replacement is required to increase α-helix propensity, as glycine is a strong α-helix breaker. We carried out the single point mutation Gly39→Ala on the Phe14→Asn mutant for use as a control for Hel2, instead of the pseudo-wild-type. Designed helix 3 (Hel3) has only the mutation Thr71→Arg (Fig. 1d). Designed helix 4 (Hel4) bears the mutations Lys91→Asn, Asn94→Ala, and Ile96→Leu (although this mutation involves a hydrophobic residue, its sidechain is fully exposed to the solvent and the hydrophobicity is conserved as they are stereoisomers; Fig. 1e). Designed helix 5 (Hel5) bears the mutations Thr115→Glu, Glu118→Lys, Asn121→Ala, and Lys122→Glu (Fig. 1f).
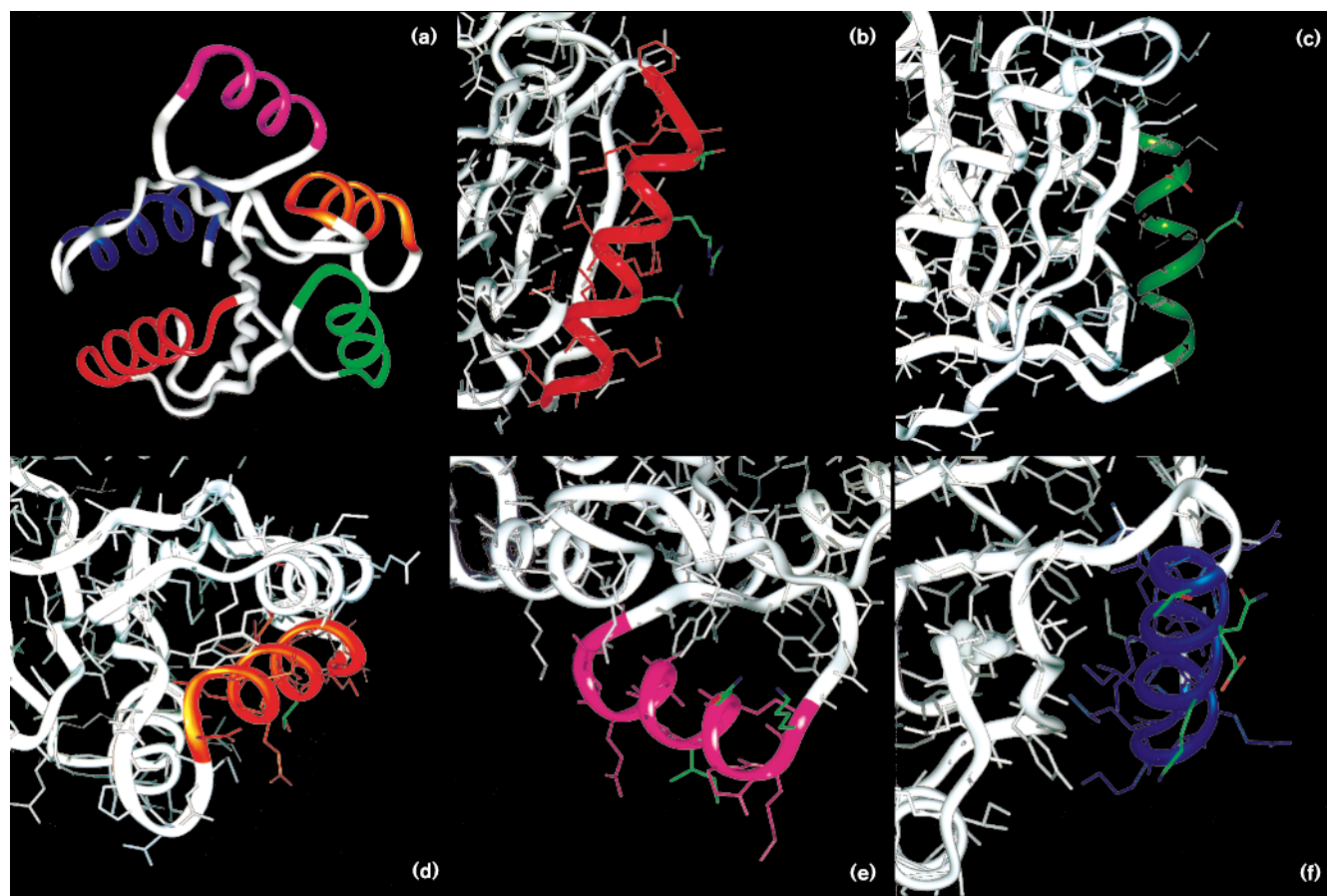
(a) Ribbon drawing depicting the three-dimensional structure of *E. coli* Che Y [23], with the five α-helices in different colours: helix 1 in red, helix 2 in green, helix 3 in orange, helix 4 in magenta, and helix 5 in blue. **(b–f)** Each of the five α-helices of Che Y showing the target sites in colour atom code and the helix with the rest of the residues in the same colour code as (a). **(b)** Helix 1, **(c)** helix 2, **(d)** helix 3, **(e)** helix 4 and **(f)** helix 5.

Evaluation of helical propensity in the enhanced α-helices

The putative increase in helical propensity produced by the mutations has been evaluated by far-UV CD analysis of peptides encompassing the isolated α-helices. In Figure 2, we show the spectra for the peptides with the wild-type and the enhanced α-helices. In all cases, an increase in helical content is observed, as indicated by more negative values of the molar ellipticity at 222 nm and shifts to higher wavelength values of the minimum ellipticity. The helical content of the peptides with wild-type and enhanced helices, calculated using the method of Chen *et al.* [26], is given in Table 1. The change in free energy for α-helix formation upon mutation of each α-helix cannot be precisely calculated using a standard two-state model. A more precise estimation can be obtained by fitting a helix/coil transition algorithm to the changes in helical content detected by far-UV CD. Such a calculation (see Materials and methods) indicates that helix 1 has been stabilized by approximately 3.68 kcal mol^{-1}, helix 2 by 1.82 kcal mol^{-1}, helix 3 by 1.68 kcal mol^{-1}, helix 4 by 1.8 kcal mol^{-1}, and helix 5 by 1.52 kcal mol^{-1}. These values have been obtained at 278 K, instead of 298 K, because the helical content is higher at this temperature and improves the resolution. This is especially important for peptides with low helical content such as those of helices 3 and 4. On the other hand, as large changes in ΔCp and ΔH between mutant and wild-type peptides are not expected, the $\Delta\Delta G$ values should be very similar at 278 and 298 K.

Thermodynamic analysis of Che Y mutants with enhanced α-helices

As a template for mutagenesis, we used a Che Y pseudo-wild-type protein containing the Phe14→Asn mutation [22]. The far-UV CD and fluorescence spectra of the six mutants (Hel1, Hel2, Gly39→Ala, Hel3, Hel4 and Hel5) are identical to those of the pseudo-wild-type protein,
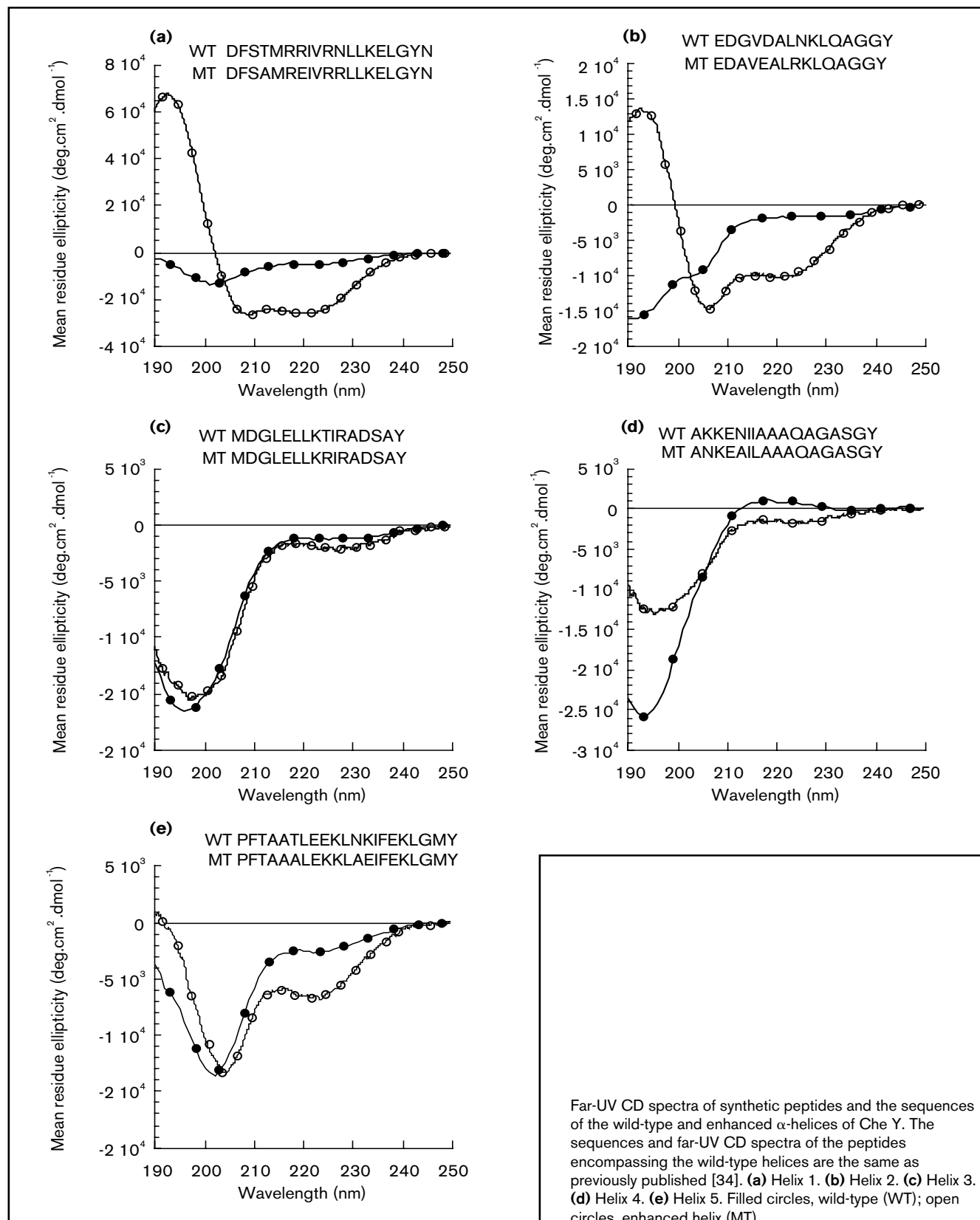
Figure 2

(a) WT DFSTMRRIVRNLLKELGYN
MT DFSAMREIVRRLLKELGYN

(b) WT EDGVDALNKLQAGGY
MT EDAVEALRKLQAGGY

(c) WT MDGLELLKTIRADSAY
MT MDGLELLKRIRADSAY

(d) WT AKKENIIAAAQAGASGY
MT ANKEAILAAAQAGASGY

(e) WT PFTAATLEEKLNKIFEKLGMY
MT PFTAAALEKKLAEIFEKLGMY

Far-UV CD spectra of synthetic peptides and the sequences of the wild-type and enhanced α-helices of Che Y. The sequences and far-UV CD spectra of the peptides encompassing the wild-type helices are the same as previously published [34]. **(a)** Helix 1. **(b)** Helix 2. **(c)** Helix 3. **(d)** Helix 4. **(e)** Helix 5. Filled circles, wild-type (WT); open circles, enhanced helix (MT).

Table 1

Helical content of the wild-type and mutant peptides.

Peptide	WT % Helix	Mutant % Helix
Helix 1	13	73
Helix 2	6	30
Helix 3	3	5
Helix 4	0	5
Helix 5	6	19

Helical population of wild-type (WT) and mutant peptides encompassing the different α-helices, determined from the ellipticity values at 222 nm [26].

both in aqueous solution and in 8 M urea (data not shown), thus indicating that the mutations do not modify the conformational properties of the folded or of the fully unfolded states. Here and throughout the manuscript, the enhanced helix 2 mutant is referenced to the Gly39→Ala mutant to eliminate the changes in thermodynamic properties produced by this single point mutation. The urea denaturation experiments, which were repeated four times on different days to determine their reproducibility, show an increase in the urea value at which half of the protein is denatured ([urea]$_{1/2}$) for the five mutants (Table 2). There is also an increase in the lower urea limit of the unfolding transition region (urea concentration at which the protein starts to unfold), as can be observed in Figure 3. Both parameters are measured directly and do not need extrapolation to aqueous conditions. This suggests an increase in protein stability for the five mutants

with enhanced α-helices. Similar results have been found in thermal denaturation experiments performed in the presence of 2 M urea to ensure reversibility [21]. This is indicated by an increase in the temperature required to half-denature the protein (Tm), which can be qualitatively assessed by observing the thermal denaturation curves shown in Figure 4. Unfortunately, these curves cannot be further analyzed here, as the thermal denaturation of Che Y in 2 M urea involves a reversible endothermic dimerization [21] (the second transition of the curves in Fig. 4). Moreover, the mutations in the α-helices appear to affect this reversible dimerization in different ways. Therefore, it is not possible to derive the thermodynamic parameters, although as stated above it is clear that the mutants are more resistant to temperature denaturation than the wild type.

Besides the increase in half urea, the urea denaturation curves show a clear decrease in the slope *m* for all the mutants (Table 2, Fig. 3). These curves are not affected by dimerization. Therefore, this means that the urea unfolding transitions are less sensitive to chemical denaturants. The observed changes in *m* do not correlate with half urea changes (data not shown). Lack of correlation rules out the possibility that the changes in the *m* value are simply a by-product of a non-linear urea dependence of the ΔG_{F-U} in the wild-type protein, as has been found recently for barnase [27]. The difference in free energy of unfolding in water ($\Delta G_{F-U}^{H_2O}$) has been calculated, with the linear extrapolation method, from the values of half urea and *m* obtained from the fitting of the unfolding transitions to a two-state model (Table 2). The changes in free energy produced by enhancement of helical propensity

Table 2

Thermodynamic and kinetic parameters of the different proteins.

| Mutant	([urea]$_{1/2}$)$_{eq}$*	m_{eq}†	ΔG_{eq}‡	([urea]$_{1/2}$)$_k$§	m_{ku}**	m_{kf}††	m_k‡‡	ΔG_{ki}§§
F14→N	4.68	1.79±0.05	8.4±0.2	4.68	0.49±0.02	−1.24±0.02	1.73±0.03	8.4±0.3
Hel1	4.86	1.52±0.05	7.4±0.2	4.92	0.46±0.02	−1.00±0.02	1.46±0.03	7.3±0.2
Hel3	5.35	1.55±0.03	8.3±0.3	5.74	0.48±0.03	−1.05±0.02	1.53±0.04	8.8±0.3
Hel4	5.39	1.67±0.05	9.0±0.3	5.51	0.49±0.03	−1.16±0.02	1.65±0.03	9.3±0.3
Hel5	5.65	1.62±0.06	9.2±0.4	5.88	0.52±0.05	−1.08±0.04	1.60±0.07	9.5±0.5
G39→A	4.42	1.69±0.03	7.5±0.2	4.52	0.55±0.02	−0.91±0.03	1.46±0.04	6.6±0.3
Hel2	4.77	1.51±0.03(0.18)	7.2±0.1(0.3)	4.90	0.56±0.01	−0.76±0.03	1.32±0.04(0.14)	6.3±0.3(0.3)

*Urea concentration at which half of the protein is denatured as measured in equilibrium. †Slope of the equilibrium denaturation curves in kcal mol M^{-1}. ‡Free energy in kcal mol^{-1} of unfolding in water, obtained by fitting the curves to a two-state transition, as indicated in Filimonov *et al.* [21]. §Urea concentration at which half of the protein is denatured as measured kinetically (these values correspond to those measured from λ2 after subtracting 0.56, which is the half urea shift between equilibrium and kinetics in the pseudo-wild-type [F14→N]).

**Variation of the natural logarithm of the unfolding rate constant with urea concentration in kcal mol M^{-1}. ††Variation of the natural logarithm of the refolding rate constant with urea concentration in kcal mol M^{-1}. ‡‡Variation of the free energy of unfolding with urea concentration obtained from the kinetic data in kcal mol M^{-1}. §§Free energy of unfolding obtained from the kinetic data as indicated in equation 2. Numbers in parentheses for the Hel2 mutant correspond to the $\Delta\Delta G$ and Δm values with respect to its control, the G39→A mutant.

Figure 3
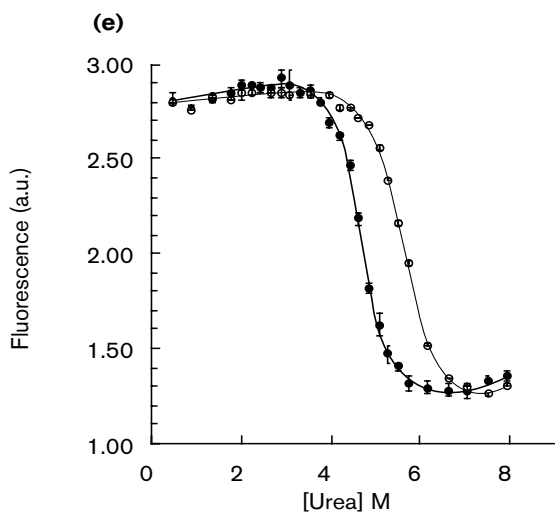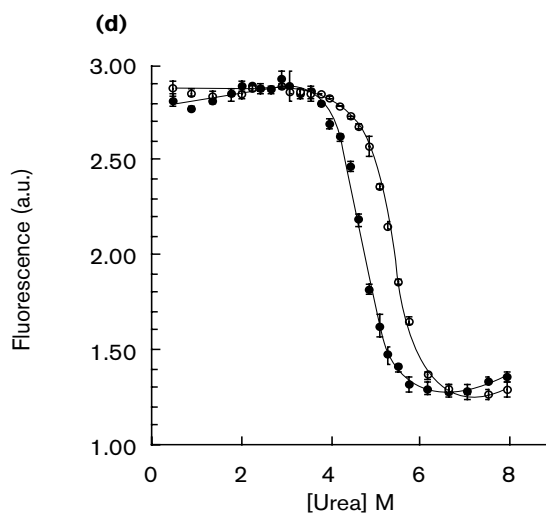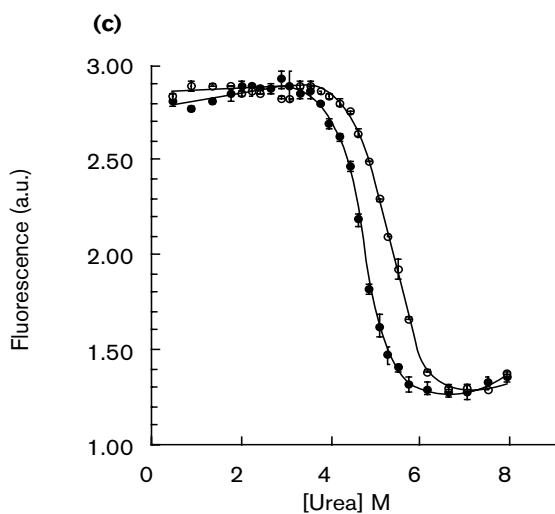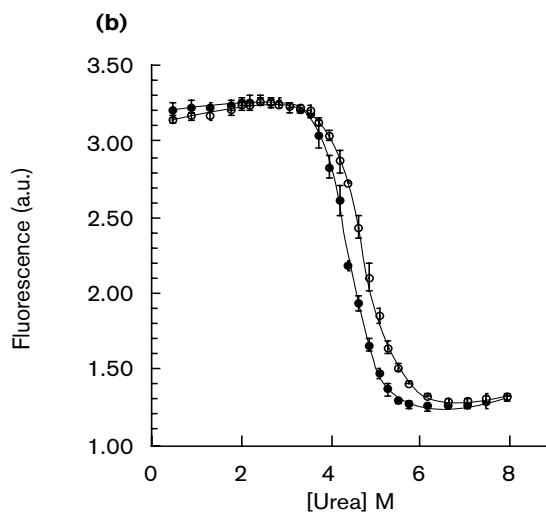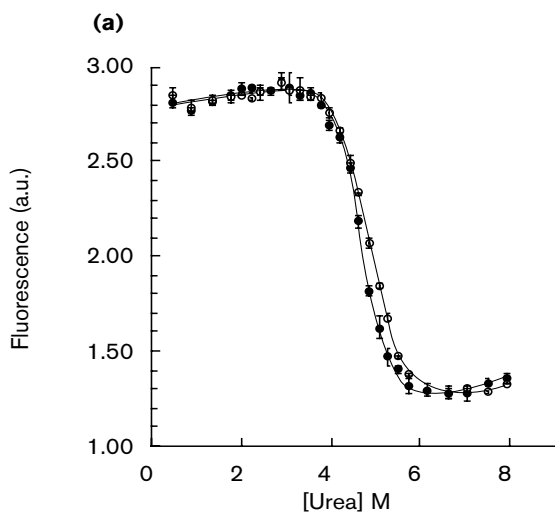
Urea-induced equilibrium denaturation curves of Che Y mutants with different enhanced α-helices. The experiment was repeated four times for each mutant and this figure shows the average values with their standard deviations. **(a)** Hel1. **(b)** Hel2. **(c)** Hel3. **(d)** Hel4. **(e)** Hel5. Filled circles, pseudo-wild-type; open circles, enhanced α-helix mutants.

Figure 4
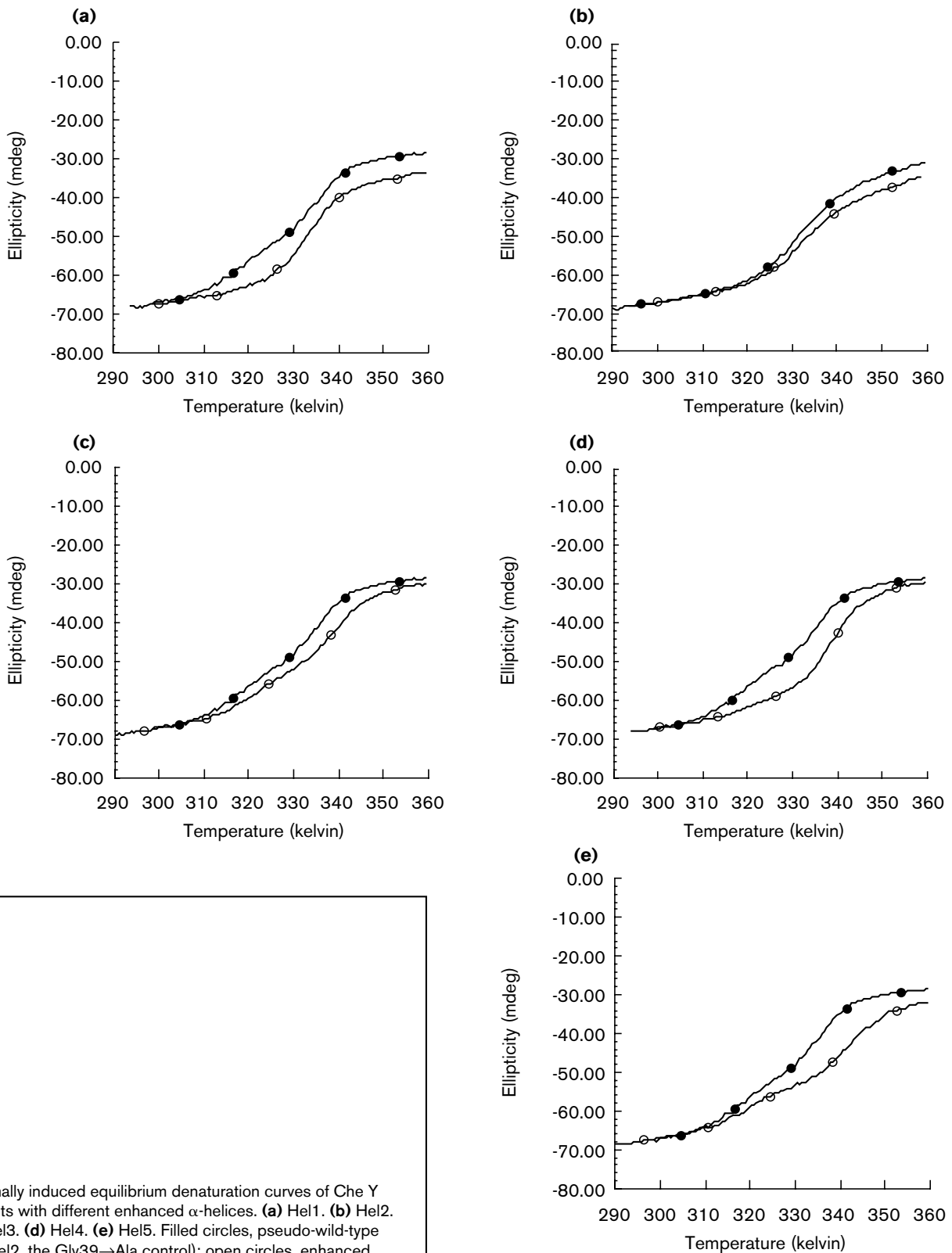
Thermally induced equilibrium denaturation curves of Che Y mutants with different enhanced α-helices. **(a)** Hel1. **(b)** Hel2. **(c)** Hel3. **(d)** Hel4. **(e)** Hel5. Filled circles, pseudo-wild-type (for Hel2, the Gly39→Ala control); open circles, enhanced α-helix mutants.

($\Delta\Delta G_{M-WT}$) vary among the mutants, ranging between the clearly negative value for Hel1 to positive values for Hel4 and Hel5 (Table 2). This is a consequence of the balance between the two opposite effects: the increase in half urea and the decrease in m.

ANS binding assays have been performed in the same experimental conditions that detected the existence of an intermediate populating the equilibrium unfolding transition of the wild-type Che Y [21]. They indicate that this intermediate is not significantly populated in the pseudo-wild-type (Fig. 5). This result is in agreement with the previous finding that the Phe14→Asn mutation significantly destabilizes the kinetically detected intermediate of Che Y [22]. Thus, the ANS binding assays are sensitive to the presence of a Che Y intermediate. Hel2 and its control (the Gly39→Ala mutant) bind ANS, but the identical value for the integral of their ANS fluorescence versus urea plots suggests that ANS binding is uniquely induced by the Gly39→Ala mutation (Fig. 5). The mutants for the other four helices do not bind ANS significantly, with perhaps the exception of Hel1 (Fig. 5).

Kinetic analysis of Che Y mutants with enhanced α-helices

Folding/unfolding kinetic analysis has been carried out to determine whether the equilibrium unfolding transitions of the mutants follow a two-state mechanism. In wild-type Che Y and all its mutants, the logarithm of the unfolding rate constant depends linearly on urea concentration. The same is true for the logarithm of the refolding rate con-

stant up to 3 M urea, though at lower urea concentrations it deviates from linearity. The kinetic parameters obtained from the fitting of the kinetic data between 3 M and 10 M urea to a two-state transition have been used to derive equilibrium parameters (see Materials and methods) that can be compared directly to those measured in equilibrium. The consistency between the two sets of thermodynamic parameters is indicative of the proteins having a two-state behaviour in equilibrium. In Table 2, both sets of parameters are given together with the original kinetic slopes. It can be observed that for the pseudo-wild-type Che Y, there is consistency between the two sets. The same is seen for Hel1, Hel3, Hel4, and Hel5. Some changes in stability, within error limits, are observed kinetically and in equilibrium (Table 2) and the differences in m are caused by changes in the urea dependence of the refolding rate constant (m_{kf} values). The Gly39→Ala control clearly deviates from a two-state behaviour, at least kinetically, as can be appreciated from the lack of correlation between the equilibrium and kinetic ΔG and m values (see Table 2). The deviation from a two-state behaviour observed for Hel2 seems to be produced only by the Gly39→Ala mutation, as indicated by the correspondence of its thermodynamic parameters calculated kinetically and in equilibrium when referenced to the Gly39→Ala values ($\Delta\Delta G$ and Δm) (Table 2). Finally, the slope of the natural logarithm of the unfolding rate constant (m_{ku}) does not change upon mutation in the five mutants with respect to their reference proteins (Table 2).

Discussion
Energetic determinants of the enhancement of Che Y α-helices

The five Che Y α-helices have been enhanced in their helical propensity by mutating several residues of their sequences. The effect of these mutations on α-helix stability is a complex balance between the introduction of attractive interactions and the removal of repulsive interactions. All these interactions are between residues that are close in the sequence (local interactions) and within the α-helix. It is possible, however, to dissect the major factors contributing to the enhancement of helical propensities using our current knowledge of α-helix stability [28]. In summary, the helical propensity has been enhanced by four types of energetic determinants. First, an increase in the intrinsic helical propensity of the residue occupying a helical position. This is found in the majority of mutations to some extent; nevertheless, some other mutations reduce the intrinsic propensity (Arg19→Glu in Hel1 and Lys122→Glu in Hel5). Second, sidechain–sidechain (i,i+3 and i,i+4) electrostatic interactions. The increases in helical propensity are found when repulsive interactions are removed or attractive interactions introduced or both simultaneously. This factor is the most important for the stabilization of helices 1, 3 and

Figure 5
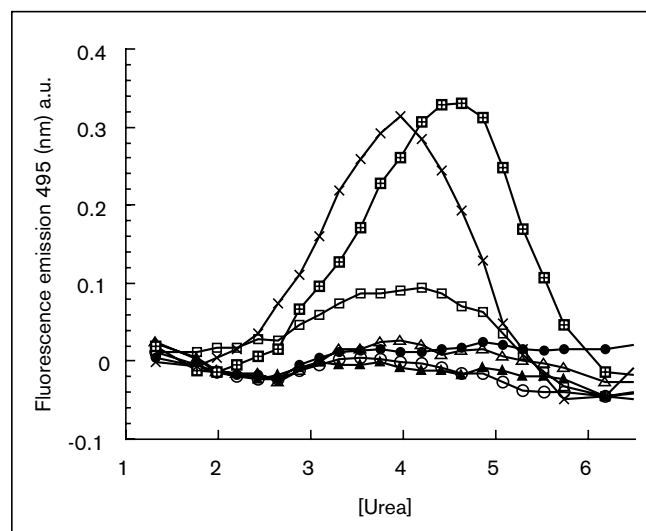
ANS binding assays for wild-type Che Y and the enhanced α-helix mutants. Open circles, pseudo-wild-type; open squares, Hel1; open triangles, Hel3; filled circles, Hel4; filled triangles, Hel5; crosses, Gly39→Ala mutant (Hel2 control); crossed squares, Hel2.

5 and also exists in helix 2. Third, better N-capping (Lys91→Asn in Hel4) or formation of a capping box motif introducing a glutamic acid at position i+3 from the N-cap (Asp41→Glu in Hel2) [29]. Fourth, interactions with the helix macrodipole, which is an important factor in Hel1 (Arg19→Glu).

Effect of the enhancement of helical propensities in the thermodynamic properties of Che Y

The effects we observe in Che Y upon enhancing the helical propensity of its α-helices are complex. One characteristic observed for all the mutants is a shift of the unfolding transition midpoint in the direction of higher denaturing conditions (increases in half urea and Tm). This means that the mutant proteins require a higher proportion of denaturing agents (chemical denaturants and temperature) than the pseudo-wild-type to be half denatured, which is indicative of stabilization. The other common characteristic for the mutants is a decrease in the sensitivity to chemical denaturants, observed as a decrease in *m*. Changes in this parameter upon mutation frequently arise from changes in hydrophobicity and/or protein packing. In this case, these can be excluded through our design strategy. An alternative explanation for the decrease in *m* is the stabilization of a partly folded intermediate, inasmuch as the equilibrium unfolding transition does not follow a two-state but rather a three-state mechanism. This has recently been found to be the case for buried Gly→Ala mutations in helix B of apomyoglobin [30]. However, our results indicate that mutants Hel1, Hel3, Hel4, and Hel5 can be considered to have a two-state unfolding transition in equilibrium, as indicated by the consistency between the thermodynamic parameters measured at equilibrium and those calculated from the folding/unfolding kinetic analysis in the 3–10 M urea range. This is further supported by the lack of ANS binding (or very weak binding in the case of Hel1) shown by these mutants in assays that are sensitive to the detection of the intermediate of wild-type Che Y (not in the pseudo-wild-type Phe14→Asn). Hel2 shows ANS binding and its kinetics and equilibrium thermodynamic parameters are inconsistent. Nevertheless, both effects appear to be produced by the mutation of the buried Gly39→Ala that has been used as its control and not by the enhancement of α-helix propensity. The effect of Gly39→Ala is the stabilization of the partly folded intermediate, similar to that described for these types of mutation in apomyoglobin [30]. Another possible explanation for the decrease in *m* found in the mutants with enhanced α-helices is that the variation in *m* arises from changes in the conformational properties of either the native state or the denatured state. The native state seems to be the same for all the mutants and for the pseudo-wild-type, as indicated by the identical far-UV CD and fluorescence spectra of all the proteins in aqueous solution. The denatured state in 8 M urea also shows identical far-UV CD and fluorescence

Table 3

Comparison between the ellipticity at 222 nm in the 2 M urea-thermally denatured state of the mutants and the increase in helical content for the corresponding peptides.

Mutant	ΔEllipticity$_{222}$(Mut–WT)*	ΔEllipticity$_{222}$(Mut–WT)†
Hel1	−19964	−710
Hel2	−8165	−629
Hel3	−341	−194
Hel4	−2515	−113
Hel5	−3882	−484

The values shown are the differences in mean residue ellipticity (deg cm^2 dmol^{-1}) at 222 nm. *Between the mutant and wild-type synthetic peptides (see Table 1). †Between the mutant and pseudo-wild-type (Phe14→Asn) proteins at 360 K.

spectra for the pseudo-wild-type and mutant proteins. However, the thermally denatured state shows a decrease in the far-UV CD signal at 222 nm in all of the mutants (Table 3, Fig. 4). Such a decrease in the ellipticity is indicative of a higher proportion of helical structure in the thermally denatured state. Furthermore, this decrease is approximately proportional to the increase in helical propensity upon mutation detected in the short peptides (see Table 3).

The simplest interpretation of these observations is based on the heteropolymer theory [31] and implies that the Che Y urea-induced unfolding transition follows a variable two-state model. Such a model seems to apply to the denaturation of the staphylococcal nuclease, a protein that shows large changes in *m* upon mutation [32]. A variable two-state model assumes that addition of a denaturing agent produces a two-state transition from the native to the denatured state, together with a change in the average properties of the denatured state. This change is gradual until it reaches a plateau at high denaturant concentrations. Such an effect comes from the shift from poor-solvent to good-solvent conditions, which is concomitant with the increase in denaturant concentration. Therefore, the denatured state is compact in aqueous solution and shifts to a more random coil conformation (the fully unfolded state) at very high denaturant concentrations. In this model, the unfolding transition is two-state-like, but the measured sensitivity to denaturant is less pronounced than in a standard two-state transition. Che Y and its Phe14→Asn mutant have, in fact, smaller experimental *m* values than expected from their size [21], which suggests that Che Y, in the denatured state, is not completely unfolded.

On the basis of the variable two-state model and our results, the smaller *m* values of the Che Y mutants arise from the compaction of the denatured state. The com-

paction is most pronounced in aqueous solution and is not observed in 8 M urea, as at this point the urea dependence of the denatured state is in plateau and the denatured state is fully unfolded. However, the compaction is observed in the thermally denatured state in the presence of 2 M urea (Fig. 4). This interpretation is further supported by the fact that the changes in m are found kinetically in the refolding reaction (m_{kf}). The compaction of the denatured state would reduce the apparent cooperativity of the urea-induced unfolding transition, as we observe, because it is measured at intermediate urea concentrations. Based on this interpretation, the ANS binding assays suggest that the compact denatured state has much lower affinity for ANS than the partly folded intermediate. This idea is supported by the fact that in the unfolding transition region of the five helix-enhanced mutants, a decrease in m is observed but not significant ANS binding, with the exception of some binding for Hel1 (the mutant with the largest decrease in m, see Table 2). On the other hand, in the Gly39→Ala mutant, in which the intermediate has been stabilized as shown by kinetics, the change in m is small but there is significant ANS binding. This is not surprising, as the compact denatured state is more heterogeneous than the partly folded intermediate and ANS is supposed to bind to definite patches of hydrophobic residues [33]. Finally, an important issue is the physical origin of the compaction of the denatured state by the enhancement of helical propensities. A possible explanation is that it comes from the restriction in the rotational freedom of the ϕ and ψ dihedral angles produced by the enhancement of helical propensities. The dihedral angles become more restricted to the α-region and this increases the rigidity of the polypeptide chain, decreases the conformational entropy of the denatured state and shifts the statistical distribution of denatured conformations to a more compact average.

In summary, the enhancement of helical propensities appears to increase protein stability at high denaturant proportions (higher half ureas and Tm) and to make more compact the denatured state. It is important, however, to determine the final effect on protein stability in aqueous solution. The free energy of unfolding in aqueous solution (ΔG_{H2O}) for each mutant has been calculated with the linear extrapolation method (Table 2) and, therefore, it arises from the balance between these two conflicting effects. The observed change in free energy upon mutation ($\Delta \Delta G_{M-WT}$) depends on which of the two effects predominate for each mutant. For mutants Hel4 and Hel5, the increase in half urea is larger than the decrease in m and the mutants are more stable than the pseudo-wild-type, with a maximal increase in stability of 0.8 kcal mol^{-1} (Table 2). In Hel2 and Hel3, the changes in both parameters basically cancel out, rendering values of $\Delta \Delta G_{M-WT}$ that are close to zero. Finally, in Hel1, the decrease in m predominates and the mutant is less stable in water than

the pseudo-wild-type (Table 2). Nevertheless, it is necessary to point out that for a variable two-state model the values of ΔG_{H2O} calculated with the linear extrapolation method, especially when m changes, are prone to error. The error arises because m is assumed to be invariant with urea in order to extrapolate from intermediate urea concentrations to water. This tends to overestimate ΔG_{F-U} because the compaction of the denatured state is more severe in water than at intermediate urea concentrations. The overestimation of ΔG_{F-U} is more important the more compacted the denatured state, so the $\Delta \Delta G_{M-WT}$ values are also overestimated because the denatured state is more compacted in the mutants than in the pseudo-wild-type. This indicates that the $\Delta \Delta G_{M-WT}$ can be smaller than we have been able to measure. On the other hand, better estimates of $\Delta \Delta G_{M-WT}$ could be obtained near the midpoint of the unfolding transition, but in this case we would be overlooking the compaction of the denatured state.

The role of local interactions in protein stability

Theoretical analyses [6] and computer simulations with simplified models of proteins [8] both indicate that the major issue in attaining a definite three-dimensional structure and optimizing protein stability is the specificity of the interactions for the native conformation. This is because protein stability results from a precise balance between the contributions stabilizing the native state and those stabilizing the rest of the conformational ensemble. In fact, it has been proposed that local interactions must be weak as they lack specificity because of their short range [6,8]. In our experiment, we have specifically increased the contribution of local interactions to the stability of Che Y. The measured increase in protein stability is in all cases much smaller than the increase in free energy for α-helix formation in the peptides. Such an effect can be more pronounced taking into account the putative overestimation of $\Delta \Delta G_{M-WT}$ mentioned above. Furthermore, we find a clear destabilization in the mutant Hel1, which corresponds to the most enhanced α-helix. Moreover, the compaction of the denatured state in all of the mutants indicates that, besides the native state, other conformations have been stabilized by enhancing helical propensities. All of this agrees with the theoretical predictions and supports the idea that optimizing protein stability and cooperativity involves achieving an optimal ratio of local versus non-local interactions. Our results suggest that natural proteins must not have a very high contribution of local interactions to be stable and cooperatively folded — explaining, perhaps, why natural proteins do not have high secondary structure propensities compared to that attainable with synthetic peptides. The implications for *de novo* protein design are also important. Designing sequences with high secondary structure propensities, seeking to ensure the formation of the desired secondary structure elements, seems to be a poor design strategy.

Materials and methods

Circular dichroism of peptides

CD spectra were acquired in a JASCO-710 dichrograph, using the continuous mode with 1 nm bandwidth, 1 s response and a scan speed of 50 nm min⁻¹. 25 scans were accumulated to obtain the final spectra. The samples were prepared in 10 mM phosphate buffer pH 7 and the experiments carried out at 278 K. Peptide concentration was determined by the absorbance at 280 nm [26], and the spectra were obtained at 10 μM peptide concentration in a 0.5 cm pathlength cuvette. Aggregation was tested as previously described [34].

Calculation of the stabilization of α-helices with a helix/coil transition algorithm

The difference in free energy for α-helix formation ($\Delta\Delta G_{Hel}$) between the pseudo-wild-type and mutated peptides was calculated from their differences in helical content as measured by far-UV CD. The algorithm for the helix/coil transition AGADIRms (V Muñoz, L Serrano, unpublished data; see Results; AGADIR is available on http://www.embl-heidelberg.de/~serrano) was used to fit the far-UV CD data of the peptides to polyalanine sequences with the same length as the peptides encompassing the α-helices of Che Y. The fitting was carried out by modifying the intrinsic propensity of alanine, maintaining the mean residue enthalpic contribution (ΔG hydrogen bond) at a constant value of −0.794 kcal mol⁻¹, to reproduce the helical content showed by the wild-type and the mutated peptides. This procedure is intended to eliminate assumptions on the individual energy contributions and on the distribution of helicity throughout the peptide. We do not have experimental information to infer them and we are interested only in the net difference in free energy for α-helix formation between wild-type and enhanced peptides. The net change in free energy for α-helix formation is finally obtained from the difference in alanine intrinsic propensity between the wild-type and mutated peptides as indicated in equation 1, where n is the peptide length:

$$\Delta\Delta G_{Hel} = \sum_{}^{n-2} (\Delta G_{intri\ MUT} - \Delta G_{intri\ WT}) \qquad (1)$$

Urea denaturation curves

The urea denaturation experiments were carried out as previously described [21]. The unfolding reaction was monitored by recording the fluorescence emission at 315 nm upon excitation at 290 nm in an AB2 SLM Aminco-Bowman spectrofluorometer. Experimental data from four different experiments performed on different days were averaged and the average fitted to equation 2:

$$F = \frac{\{(F_N + a\ [\text{denat.}]) + (F_U + b\ [\text{denat.}])\ \exp(m\ [\text{denat.}] - \Delta G_{H_2O})\ /\ RT\}}{\{1 + \exp(m\ [\text{denat.}] - \Delta G_{H_2O})\ /\ RT\}}$$
$$(2)$$

where F is the fluorescence emission of the protein, F_N is the fluorescence of the folded state and F_U of the unfolded state. The dependence of the intrinsic fluorescence upon denaturant concentrations, in both the native and the denatured states, is taken into account by the terms of a [urea] and b [urea], respectively, where a and b are constants. To obtain good estimates of b, especially in mutants with large half ureas, we measured the fluorescence of the protein in the range 7.5–9.0 M urea at intervals of 0.25 M and fitted them to a straight line. The values from this fitting were introduced as constant parameters in the global fitting with equation 2. In Hel3, Hel4 and Hel5, the constant a was set to zero to account for their lack of fluorescence dependence on the folded state.

Thermal denaturation experiments

The thermally induced unfolding transitions for the pseudo-wild-type and the different mutants were performed in 2 M urea, 50 mM Na₂PO₄, pH 7. Urea was added to make reversible the dimerization of the intermediate occurring in the thermal denaturation of Che Y [21]. The unfolding transition was followed by far-UV CD at 222 nm on a JASCO-710 dichrograph, using the continuous mode with 1 nm bandwidth, 1 s response and a thermal ramp of 50°C h⁻¹. Protein concentration was in all the cases 88 μM in a cuvette with 0.2 cm pathlength. Thermal denaturation reversibility was checked by comparing the far-UV CD spectra of the protein at the beginning of the experiment and after cooling it down to the initial temperature (278 K). The concentration dependence of the thermally induced unfolding was checked by comparison with the results obtained in the 88–5 μM range.

ANS binding assays

ANS binds to patches of hydrophobic residues exposed to the solvent and this is used to detect the existence of partly folded intermediates [33]. The experiments were carried out using an AB2 SLM Aminco-Bowman spectrofluorometer in 50 mM Na-PIPES, pH 7, at the same urea concentrations as in the equilibrium denaturation experiments. In all cases, we added ANS to 250 μM final concentration and 20 μM protein (ratio 12:1). The excitation wavelength was 396 nm and the emission signal was recorded at 495 nm. The temperature was kept constant at 298 K.

Kinetic experiments

The kinetic measurements were carried out as previously described for the pseudo-wild-type and Phe14→Asn mutant [22]. Che Y and its mutants studied here have a *cis* prolyl residue that produces the observation of two macroscopic rate constants ($\lambda 1$ and $\lambda 2$), the fast phase corresponding to the folding of the population with the prolyl residue in *cis* conformation [35]. The fast phase ($\lambda 2$) was studied with a Bio-Logic stopped-flow machine (SFM3) coupled to a Bio-Logic modular optical system. Changes in fluorescence emission were monitored by exciting at 290 nm and recording fluorescence emission with a 305 nm cut-off filter.

Analysis of kinetic data

In the pseudo-wild-type (Phe14→Asn), the logarithm of the fast refolding reaction depends linearly on the urea concentration within the range 3–5 M urea [22]. The calculation of the kinetic parameters using a two-state model was carried out for all the proteins with only the refolding values within the linear region (3–5 M urea). We fitted the values of $\lambda 2$ at urea concentrations higher than 3 M to equation 3:

$$\ln\{k_{f,H_2O}{}^* \exp(-m_{kf}{}^*[\text{urea}]/RT) + k_{u,H_2O}{}^* \exp(-m_{ku}{}^*[\text{urea}]/RT)\} \qquad (3)$$

where k_{f,H_2O} is the rate constant of refolding in water, m_{kf} is the variation of the natural logarithm of the refolding rate constant with urea concentration, k_{u,H_2O} is the rate constant of unfolding in water, and m_{ku} is the variation of the natural logarithm of the unfolding rate constant with urea concentration.

The thermodynamic parameters were calculated from the kinetic parameters by equations 4 and 5:

$$\Delta G_{F,U} = -RT \ln (k_{f,H_2O} / k_{u,H_2O}) \qquad (4)$$

$$m = m_{ku} - m_{kf} \qquad (5)$$

The $\Delta G_{F,U}$ calculated kinetically from $\lambda 2$ is higher than the value at equilibrium because of the neglect of the slow phase produced by the isomerization of the *trans* prolyl residue in the unfolded state [35]. This effect has been calculated in the Phe14→Asn mutant from the shift between the half urea value measured kinetically from the fast phase and in equilibrium as 1.0 kcal mol⁻¹ (results from a population of 15.5% unfolded molecules with the prolyl residue in *cis* conformation). As this contribution is only due to the *trans/cis* prolyl isomerization in the unfolded state [35], it can be assumed constant with mutations that do not involve the *cis* prolyl residue. We have used for all the mutants a constant value of 1.0 kcal mol⁻¹ to account for this effect on the $\Delta G_{F,U}$ values calculated kinetically.

References

1. Tanford, C. (1968). Protein denaturation. *Adv. Protein Chem.* **23,** 121–282.
2. Jaenicke, R. (1991). Protein folding: local structures, domains, sub-units, and assemblies. *Biochemistry* **30,** 3147–3161.
3. Dill, K.A. (1990). Dominant forces in protein folding. *Biochemistry* **29,** 7133–7155.
4. Sauer, R.T. & Lim, W.A. (1992). Mutational analysis of protein stability. *Curr. Opin. Struct. Biol.* **2,** 46–51.
5. Fersht, A.R. & Serrano, L. (1993). Principles of protein stability derived from protein engineering experiments. *Curr. Opin. Struct. Biol.* **3,** 75–83.
6. Dill, K.A., *et al.*, & Chan, H.S. (1995). Principles of protein folding – a perspective from simple exact models. *Protein Sci.* **4,** 561–602.
7. Dill, K.A., Fiebig, K.M. & Chan, H.S. (1993). Cooperativity in protein folding kinetics. *Proc. Natl. Acad. Sci. USA* **90,** 1942–1946.
8. Thomas, P.D. & Dill, K.A. (1993). Local and non-local interactions in globular proteins and the mechanism of alcohol denaturation. *Protein Sci.* **2,** 2050–2065.
9. Rey, A. & Skolnick, J. (1993). Computer modelling and folding of four-helix bundles. *Proteins* **16,** 8–28.
10. Muñoz, V. & Serrano, L. (1994). Elucidating the folding problem of helical peptides using empirical parameters. *Nat. Struct. Biol.* **1,** 399–409.
11. O'Neil, K. & DeGrado, W.A. (1990). A thermodynamic scale for the helix-forming tendencies of the commonly occurring amino acids. *Science* **250,** 246–250.
12. Horovitz, A., Matthews, J.M. & Fersht, A.R. (1992). α-Helix stability in proteins. II. Factors that influence stability at an internal position. *J. Mol. Biol.* **227,** 560–568.
13. Blaber, M., Zhang, X. & Matthews, B.W. (1993). Structural basis of amino acid α-helix propensity. *Science* **260,** 1637–1640.
14. Kim, C.A. & Berg, J.M. (1993). Thermodynamic β-sheet propensities measured using a zinc-finger host peptide. *Nature* **362,** 267–270.
15. Minor, D.L. & Kim, P.S. (1994). Measurement of the β-sheet forming propensities of the amino acids. *Nature* **367,** 660–663.
16. Smith, C.K., Withka, J.M. & Regan, L. (1994). A thermodynamic scale for the β-sheet forming tendencies of the amino acids. *Biochemistry* **33,** 5510–5517.
17. Mitchinson, C. & Baldwin, R.L. (1986). The design and production of 3 ribonucleases with increased thermostability by incorporation of S-peptide analogues with enhanced helical stability. *Proteins* **1,** 23–33.
18. Lin, L., Pinker, R.J., Phillips, G.N. & Kallenbach, N.R. (1994). Stabilization of myoglobin by multiple alanine substitutions in helical positions. *Protein Sci.* **3,** 1430–1435.
19. Blaber, M., Baase, W.A., Gassner, N. & Matthews, B.W. (1995). Alanine scanning mutagenesis of the α-helix 115–123 of phage T4 lysozyme: effects on structure, stability and the binding of solvent. *J. Mol. Biol.* **246,** 317–330.
20. Muñoz, V. & Serrano, L. (1995). Elucidating the folding problem of helical peptides using empirical parameters. II. Helix macro dipole effects and rational modification of the helical content of natural peptides. *J. Mol. Biol.* **245,** 275–296.
21. Filimonov, V.V., *et al.*, & Serrano, L. (1993). Thermodynamic analysis of the chemotactic protein from *E. coli*, Che Y. *Biochemistry* **32,** 12906–12921.
22. Muñoz, V., Lopez, E., Jager, M. & Serrano, L. (1994). Kinetic characterization of the chemotactic protein from *E. coli*, Che Y. Kinetic analysis of the inverse hydrophobic effect. *Biochemistry* **33,** 5858–5866.
23. Volz, K. & Matsumura, P. (1991). Crystal structure of *E. coli* Che Y refined at 1.7 Å resolution. *J. Biol. Chem.* **266,** 15511–15519.
24. Kabsch, W. & Sander, C. (1983). Dictionary of protein secondary structure pattern recognition of hydrogen-bonded and geometrical features. *Biopolymers* **22,** 2577–2637.
25. Lee, B. & Richards, F.M. (1971). The interpretation of protein structures: estimation of static accessibility. *J. Mol. Biol.* **55,** 379–400.
26. Chen, Y.H., Yang, J.T. & Chau, K.H. (1974). Determination of the helix and β form of proteins in aqueous solution by circular dichroism. *Biochemistry* **13,** 3350–3359.
27. Johnson, C.M. & Fersht, A.R. (1995). Protein stability as a function of denaturant concentration: the thermal stability of barnase in the presence of urea. *Biochemistry* **34,** 6795–6804.
28. Muñoz, V. & Serrano, L. (1995). Helix design, prediction and stability. *Curr. Opin. Biotechnol.* **6,** 382–386.
29. Lyu, P.C., Zhou, H.X., Jelveh, N., Wemmer, D.E. & Kallenbach, N.R. (1992). Position-dependent stabilizing effects in α-helices: N-terminal capping in synthetic model peptides. *J. Am. Chem. Soc.* **114,** 6560–6562.
30. Kiefhaber, T. & Baldwin, R.L. (1995). Intrinsic stability of individual α-helices modulates structure and stability of the apomyoglobin molten globule form. *J. Mol. Biol.* **252,** 122–132.
31. Dill, K.A. & Shortle, D. (1991). Denatured states of proteins. *Annu. Rev. Biochem.* **60,** 795–825.
32. Shortle, D. (1994). Staphylococcal nuclease: a showcase of m-value effects. *Adv. Protein Chem.* **46,** 217–246.
33. Semisotnov, G.V., *et al.*, & Gilmanshin, R.I. (1991). Study of the molten globule intermediate state in protein folding by a hydrophobic fluorescent probe. *Biopolymers* **31,** 119–128.
34. Muñoz, V., Serrano, L., Jimenez, M.A. & Rico, M. (1995). Structural analysis of peptides encompassing all α-helices of three α/β parallel proteins: Che-Y, flavodoxin and P21-ras: implications for α-helix stability and the folding of α/β parallel proteins. *J. Mol. Biol.* **247,** 648–669.
35. Kiefhaber, T., Kohler, H.H. & Schmid, F.X. (1992). Kinetic coupling between protein folding and prolyl isomerization. I. Theoretical models. *J. Mol. Biol.* **224,** 217–229.